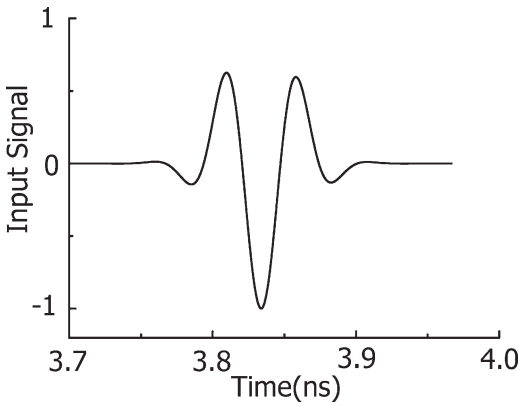

Figure 13 The input pulse in the measurement

time-domain transmission from one to another is measured in door with the Advantest R3770 Network Analyzer, which has the time-domain function. The relative orientations of them are set as the following five kinds: (a) face to face; (b) face to back; (c) back to back; (d) in the same plane, and (e) perpendicular, as drawn in Figure 12. The input signal of the radiating antenna is a modulated gauss pulse with the width of 0.3 ns and the normalized amplitude of 1, as shown in Figure 13. The measured and simulated received signals are listed in Figure 12. The measured waveforms are consistent with the simulated results basically, validating the calculations in part 3. The durations of the waveforms may come from the reflection by the cable connectors or the walls near the antenna in the measurement. Moreover, the main parts of the received signals in the five orientations maintain consistency to the input pulse of the radiating antenna except in case (a), indicating the nice pulse fidelity of the proposed antenna.

5. CONCLUSIONS

The traditional antenna parameters such as the return loss and the antenna gain are not good descriptors for the antenna used in the pulse radio UWB systems. The group delay in S_{11} cannot point out how good are the time-domain characteristics directly. The correlation coefficient can depict the fidelity of the radiated pulse but ignore the energy. For describing the comprehensive time-domain performance of the UWB antenna used in the correlation detection UWB systems, the CEG is a good descriptor. By using the MCEG as the criterion, a planar goblet-like UWB antenna is proposed and optimized successfully. The simulated and measured results show that the new designed antenna has good time-domain waveform fidelity while keeping good match performance and radiating ability.

ACKNOWLEDGMENTS

Authors would like to express their sincere thanks to Nation Nature Funding U0635004 for its financial support.

REFERENCES

1. FCC News Release, Revision of Part l5 of the Commission's Rules Regarding UWB Transmission systems, Adopted 14 February 2002, Released 22 April 2002.
2. Z.-N Chen, UWB Antennas: From Hype, Promise to Reality, LAPC 2007 Conference Proceedings, 2007, pp. 19–22.
3. Q.-X. Chu and Y.-Y Yang, A compact ultrawideband antenna with 3.4/5.5GHz dual band-notched characteristics, IEEE Trans Antennas Propag 56 (2008), 3637–3644.
4. Y.-Y Yang, Q.-X. Chu, and Z.-A Zheng, Time domain characteristics of band-notched ultrawideband antenna, IEEE Trans Antennas Propag 57 (2009), 3426–3430.
5. Y.-Q. Shi, A. Sheel, and L.-L. Choi, Time domain responses of printed UWB antennas, 2005 Fifth International Conference on Information, Communications and Signal Processing, 2005, pp. 153–156.
6. Q. Wu, R.-H. Jin, J.-P. Geng, and M. Ding, Pulse preserving capabilities of printed circular disk monopole antennas with different grounds for the specified input signal forms, IEEE Trans Antennas Propag 55 (2007), 2866–2873.
7. P. Cerny and M. Mazaneka, Simulated transient radiation characteristics of optimized ultra wideband printed dipole antennas, 2007 17th International Conference Radioelektronika, 2007, pp. 1–6.
8. J.S. McLean, H. Foltz, and R. Sutton, Pattern descriptors for UWB antennas, IEEE Trans Antennas Propag 53 (2005), 553–559.

A HYBRID STAR-RING-BUS ARCHITECTURE FOR WDM METROPOLITAN-REGIONAL ACCESS NETWORKS

Shu-Tsung Kuo,[1] Ming-Seng Kao,[1] and Peng-Chun Peng[2]
[1] Department of Electrical Engineering, National Chiao-Tung University, Hsinchu 300, Taiwan, R.O.C; Corresponding author: rogerkuo13@gmail.com
[2] Department of Electro-Optical Engineering, National Taipei University of Technology, Taipei 106, Taiwan, Republic of China

Received 16 April 2010

ABSTRACT: *This work proposes a highly reliable, hybrid star-ring-bus architecture (SRBA) for broadband wavelength-division multiplexed (WDM) regional access networks. A delta-star network on the top level acts as high-capacity trunk infrastructure, whose weakness in reliability is overcome by the self-healing function of the concatenated ring network on the lower level. The ring network is divided into several delta regions, where the traffic load inside each region is unified to minimize the backup resources required in the network. On the bottom level, considerable bus subnets are constructed to serve end users. The idea of λ-bands is introduced to efficiently manage wavelength carriers used in the network. Moreover, by means of the automatic protection switching (APS) systems in all the optical network units (ONUs), a minimum-hop rerouting protection scheme against fiber failure(s) is designed. Specifically, we carry out an experimental network to demonstrate the feasibility and survivability of the proposed architecture.* © 2010 Wiley Periodicals, Inc. Microwave Opt Technol Lett 53:102–108, 2011; View this article online at wileyonlinelibrary.com. DOI 10.1002/mop.25628

Key words: *regional access networks; star-ring-bus architecture; delta-star structure; λ-band*

1. INTRODUCTION

With the rapidly growing demands for more diverse broadband services, a flexible data-optimized access network infrastructure is required to alleviate the rising traffic load [1–3]. The wavelength-division multiplexing (WDM) technology allows tens of wavelength channels to be delivered simultaneously over a single-mode fiber in a transparent fashion, which enables a tremendous increase in the transmission capacity of an optical communication network. Accordingly, the introduction of WDM into a metropolitan-regional area access network is effectual for eliminating the bandwidth bottleneck between backbone and access networks. As the WDM scheme advances toward the end users,

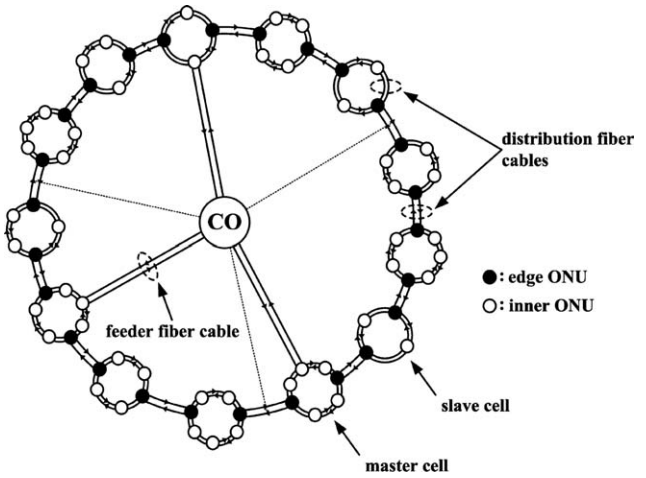

Figure 1 Upper-level star-ring network in the proposed SRBA

more and more close attention is paid to network functions and cost reductions. This generates new challenges for the topology design, wavelength management, and protection mechanism when designing high-capacity regional access networks [4–6].

The interconnection of fibers, that is, the network topology, defines lightpaths wherein a multitude of wavelengths can propagate. As lightpaths are the basic building blocks in the optical network architecture, their establishment is getting critical. To date, many regional WDM access networks are constructed in either a star or a ring topology, where both configurations have their respective virtues and drawbacks [7, 8]. To jointly keep high bandwidth efficiency and network survivability, several complementary star-ring regional access network architectures were proposed [9, 10]. However, the stars in those hybrid star-ring networks are connected to all of the deployed optical network units (ONUs). As the number of ONUs increases, the difficulty and cost in constructing such optical access networks will multiply.

Moreover, a good wavelength management scheme, which specifies how to optimally deal with wavelength channels, is another critical concern in the design of broadband access networks. In the absence of wavelength conversion, the wavelength management is subjected to the wavelength-continuity constraint—any two lightpaths at the same wavelength cannot share a physical fiber link. These issues should be seriously considered in devising WDM access networks.

This letter proposes a hierarchical access network architecture that involves three popular topologies on different levels. On the top level, several star feeder fiber cables are deployed to connect the central office (CO) with some particular rather than all component ONUs to markedly reduce the difficulty and cost in network implementation. Next, a concatenated ring network is constructed on the middle level to overcome the star's inherent weakness in reliability. In our design, the ring network is divided into several delta regions, each having the near-uniform traffic load. The interregion traffic uniformization is aimed at minimizing the hardware redundancies needed in case of fiber failure(s). On the bottom level, the bus topology is utilized to construct those subscriber loops because of its high scalability and low start-up cost. Furthermore, the special cascade add/drop transceiver (CAT) structures are connected in series in each bus subnet to compensate the up/downstream signals for branch losses, which can serve a large number of users without using any optical amplifiers.

Several techniques beneficial to the network cost reduction and reliability enhancement are jointly implemented in the proposed star-ring-bus architecture (SRBA). First, the spatial wavelength reuse for separate dual-ring subnet clusters and optical fibers is performed on the conflict-free criterion to decrease the number of specific lightwave sources used in the SRBA [11]. Second, the idea of λ-band is introduced to facilitate the wavelength management, whereby the networking complexity is much reduced. Finally, each ONU entity in this access network is equipped with an automatic protection switching (APS) system, which would be used to support the minimum-hop rerouting work for affected up and downstream traffic in case of fiber break(s) if necessary [12]. These techniques enable us to use the minimum of network resources to retain a high level of network service in normal and protection conditions.

2. NETWORK CONFIGURATION AND OPERATION

The hierarchical WDM access network based on the proposed SRBA is illustrated in Figures 1 and 2, where the former shows the upper-level star-ring network, and the latter depicts the bottom-level bus subnets. As shown in Figure 1, each delta region defined by two adjacent dashed lines contains several dual-ring subnets. Within a region, a star cable is served as the bridge between the CO and its corresponding ring subnet cluster, where each ring subnet is called a cell. The idea of cell is adopted from wireless communications, wherein a cell uses a specific frequency band to carry messages [13]. As will be clear later, a ring subnet in our approach will use a specific wavelength band (named as the λ-band) to deliver data packets; therefore, such a ring subnet is denominated as a cell to distinguish it from common ring networks.

In the proposed access network, each cell is composed of several ONUs, whose traffic is the aggregate of its ONUs' and is delivered to/from the CO via its λ-band allotment. For the ease of wavelength management, each λ-band would be managed as a sole unit on the transport route. Within a delta region, the particular cell connected to the CO directly is called the master cell and the others are the slave cells. The λ-band traffic of a cell is sent to/from the CO through the master cell of the same delta region in normal operation, or via the closest master cell in the neighboring region while being affected by a fiber break. There are several optical fibers in a feeder/distribution fiber cable. Most of them are primary fibers used for regular-traffic deliveries, and the others are backup fibers reserved for the protection purpose.

Next, as demonstrated in Figure 2, each ONU in a cell is connected with several bus subnets via A-adaptors. In addition, a series of B-adaptors are cascaded in each subnet. The A-adaptor consists of only two thin-film filters (TFFs) for wavelength adding and dropping. As to the B-adaptor, the CAT structure composed of a PIN photodetector, an electrical add-drop module and a laser transmitter is installed. The usage of CAT structures enables easy signal regeneration, allowing a nearly error-free packet delivery in the branch without using any expensive optical amplifiers. This can serve a large number of end users in a cost-effective way. Note that all the B-adaptors of a bus subnet are equipped with the Fabry-Pérot (FP) laser transmitters except for the last one being provided with the distributed feedback laser diode (DFB-LD) module, which can further reduce the expense for constructing a subnet.

An efficient wavelength management scheme using the idea of λ-band is adopted in the SRBA, and is addressed as follows. As shown in Figure 2, a bus subnet drops one specific

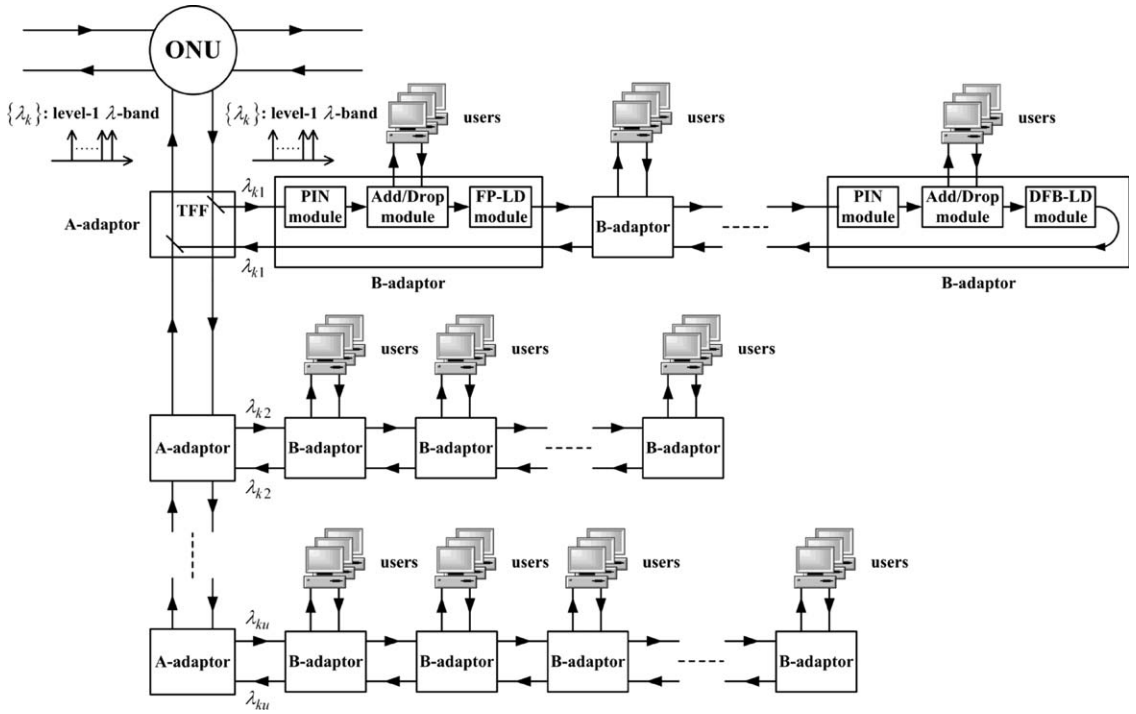

Figure 2 Bottom-level bus subnets in the proposed SRBA

wavelength λ from a particular downstream wavelength group $\{\lambda_k\}$ termed as a level-1 λ-band. For the sake of brevity, the exposition of this wavelength management scheme starts with an optical downstream packet at wavelength λ_{kj}. The optical packet is sent to the first B-adaptor of the destined subnet and is converted to electrical by its PIN photodetector. Then, this packet is forwarded to the electrical add-drop module in which the packet will be dropped or passed, depending on its destination is one of the terminals attached to this B-adaptor or not. On the other hand, the upstream packet coming from any terminal of this B-adaptor is added to the data sequence via time-division multiplexing. The output of the add-drop module is then delivered to the next B-adaptor via the FP laser transmitter. The wavelength of the FP laser transmitter can be different from that of λ_{kj}, and so are those in the other B-adaptors. The same operation is performed in the following B-adaptors in a cascade manner. As a result, all the downstream packets are received by their destination terminals, whereas all the upstream packets are eventually carried by the wavelength λ_{kj} via the DFB laser transmitter in the last B-adaptor and then sent to the ONU via the corresponding A-adaptor. Different wavelength carriers λ_{kj}'s from different bus subnets are copropagating and naturally merged together as a level-1 λ-band in the loop fiber, as illustrated in Figure 2. Afterward, the level-1λ-band is received by the ONU.

The schematic diagram of the dual-ring structure for a slave cell is depicted in Figure 3. There are two edge ONUs and several inner ONUs in the cell wherein two fiber cables are used to make neighboring ONUs which have two connections in between. The edge ONUs are constructed to manage both intercell traffic and intra-cell traffic, and the inner ONUs are responsible for intracell traffic only. Therefore, those edge ONUs are equipped with additional edge switches that are absent inside the inner ONUs. The edge switches in the edge ONUs make them able to appropriately route intercell and intracell traffic to/from the intended master cell. An APS system composed of two multiwavelength add/drop multiplexers and a λ-band switch, as

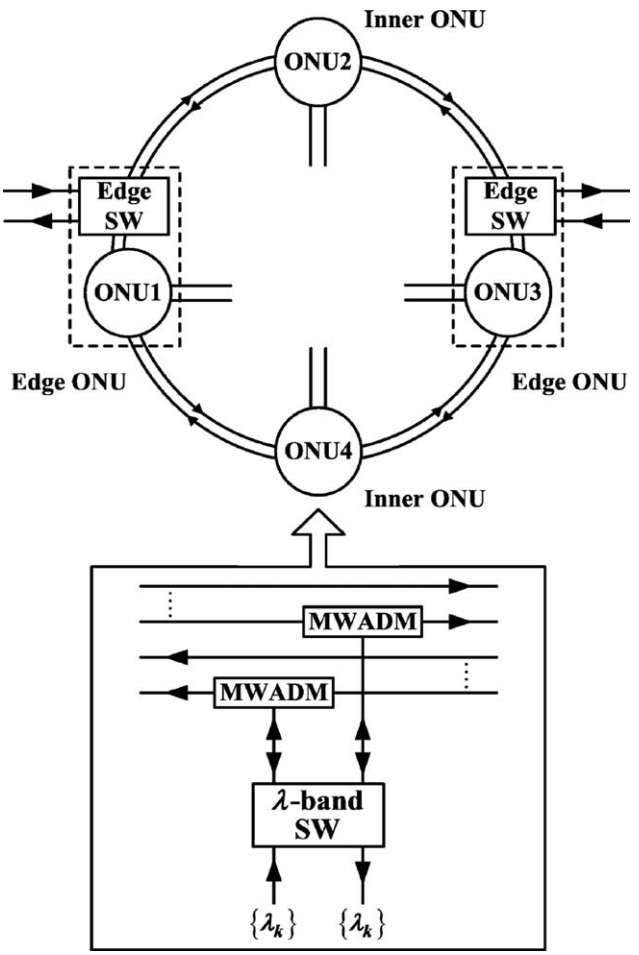

Figure 3 Configurations of a slave cell and its ONU entity

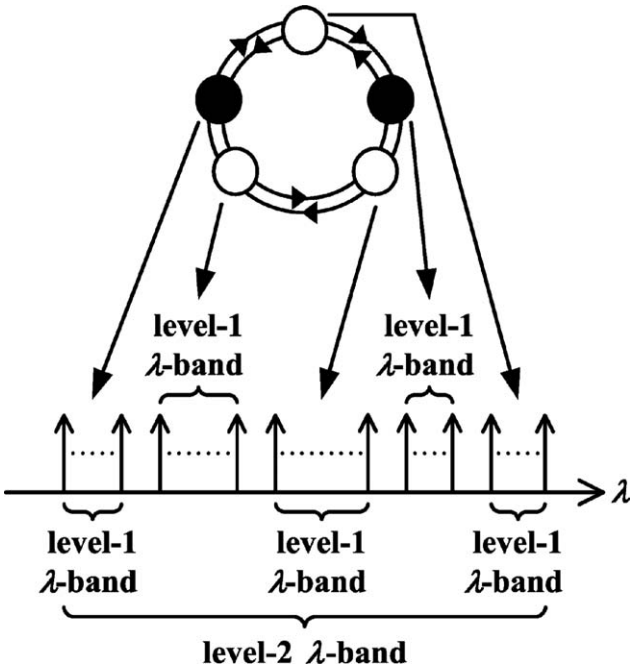

Figure 4 Illustration of level-2 λ-band formation within a slave cell

shown in the figure, is installed in each inner/edge ONU entity to protect it from fiber failure(s). Within such an ONU entity, all its transmitting/receiving wavelengths are added to/dropped from an optical fiber via the APS module in the bidirectional fashion. The APS system can work in coordination with edge switches to reroute affected λ-bands of the ONU counterpart promptly to/from the CO for different fiber failure scenarios.

Referring to Figure 3, a specific level-1 λ-band is assigned to each ONU inside a cell. Different cells may use the same or different level-1 λ-bands, but all the level-1 λ-bands in a cell are distinct. Within a slave cell, those level-1 λ-bands generated by its ONUs are all added to the identical fiber to facilitate wavelength management. They are sent to the edge ONU that is closer to the master cell of the same delta region as shown in Figure 1. Those level-1 λ-bands are naturally merged together as a level-2 λ-band in the fiber, as depicted in Figure 4. At the edge ONU, the upstream level-2 λ-band of this cell is forwarded to the next cell, and eventually through the master cell of the corresponding delta region to the CO.

On the other hand, the wavelength management of receiving λ-bands is carried out along the downstream paths, which is opposite to that in the upstream case aforementioned. First, those receiving level-2 λ-bands destined to a particular delta region are output from the CO, and received by the master cell of the delta region. Then, each level-2 λ-band is sent to the corresponding cell through the concatenated ring network. Inside a cell, the received level-2 λ-band is decomposed into several level-1 λ-bands, which are then forwarded to their respective destination ONUs accordingly. Each individual wavelength of a level-1 λ-band is sent to a specific bus subnet via the A-adaptor. Eventually, the downstream data packets are delivered to end users via B-adaptors.

Note that each λ-band in the network is managed as a sole unit on upper network levels to simplify the wavelength management—all wavelengths in a λ-band are routed and switched altogether and simultaneously. Namely, we just have to merge or decompose λ-bands in the SRBA without dealing with individual wavelengths. In our scheme, the spatial wavelength reuse for diverse λ-bands carried by separate fibers and different cell clusters in the SRBA is performed on the conflict-free criterion, which can greatly reduce the amount of specific lightwave sources used. Therefore, the wavebands applied in all the cell clusters are almost or even the same.

3. PROTECTION MECHANISM AGAINST FIBER LINK FAILURES

In the proposed hierarchical access network, the effect of a fiber failure on the bottom level is less critical than that on upper levels. To effectively prevent our network from a severe packet loss, we introduce the loop-back protection scheme against the fiber failure(s) on upper levels. With the switching systems inside a cell as shown in Figure 3, bidirectional transmissions/receptions of λ-bands can be achieved on the middle network level, and hence each of those λ-bands affected by a fiber failure can be rerouted to its destination through a backup lightpath instead of its failed primary one. The full path protection mechanism for the upper-level star-ring network will be illustrated later, which is able to restore the affected traffic promptly with minimum disturbance on the existing traffic from/to the other cells.

Three types of fiber link failures, as depicted in Figures 5(a)–5(c), are considered. The first (i.e., Type I failure) occurs in a feeder fiber cable connecting the CO and a master cell. The second (i.e., Type II failure) and the last (i.e., Type III failure) are the distribution fiber failures between two adjacent cells and within a cell, respectively. In our scheme, a cell affected by a Type I or II failure will reroute its traffic to/from the CO through the other feeder fiber cable instead of the specified one

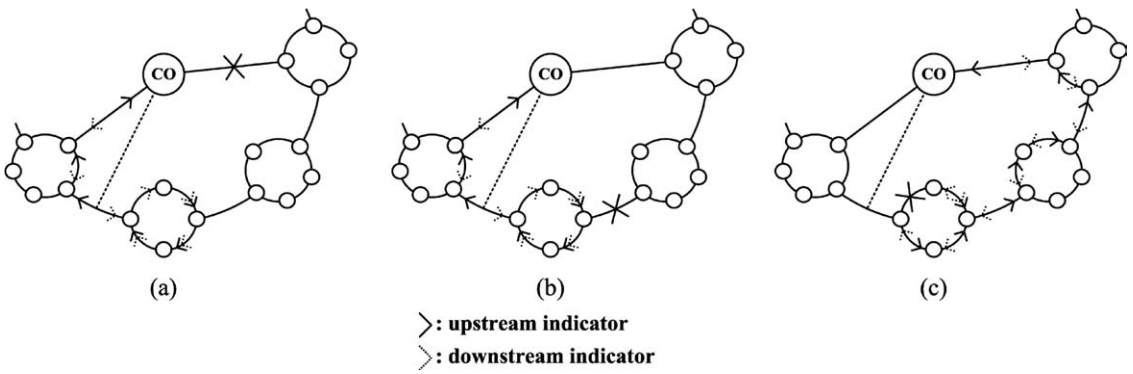

Figure 5 Three types of fiber link failures with regard to the proposed star-ring network and the up/downstream protection packet-delivery route of a cell affected by a (a) Type I, (b) Type II, or (c) Type III failure

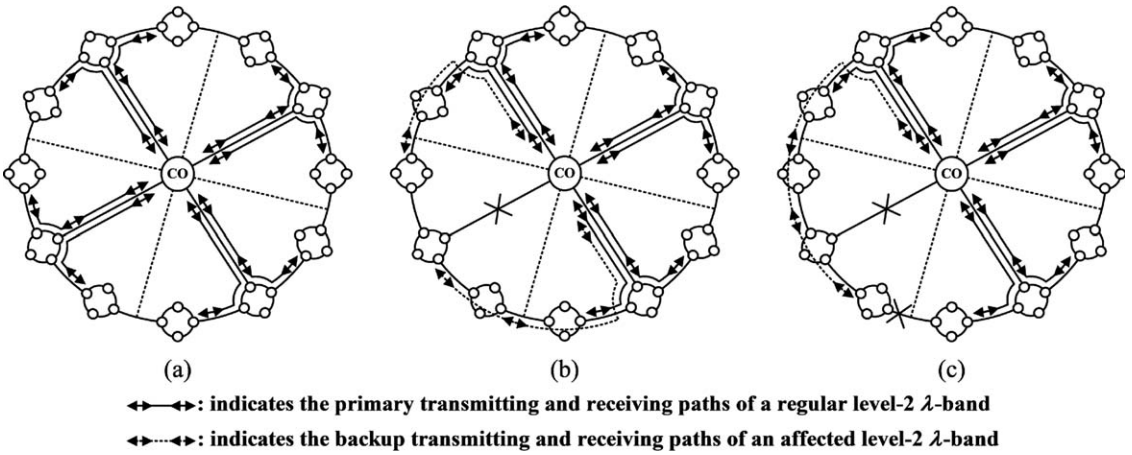

Figure 6 Operation of an illustrative star-ring network with (a) no failures, (b) one Type I failure, or (c) a Type I plus a Type II failures

in the minimum-hop detouring fashion, while the one accompanied with a Type III failure still transmits/receives its level-2 λ-bands along the original primary path. Apparently, a Type III failure leads to the least influence on the network operation.

Figure 6 schematically depicts how the loop-back protection mechanism reacts to safeguard our network against different fiber failure scenarios. In this figure, the primary and backup transmitting/receiving paths of a regular and an affected level-2 λ-bands are indicated by the four-arrow-headed solid and dashed lines, respectively. Note that those dashed lines are given by following the criterion of minimum-hop rerouting. The first case shown in Figure 6(a) demonstrates the network in normal operation. The second and the third depicted in Figure 6(b) and 6(c) present the network works under the attacks of a single Type I failure and a Type I plus a Type II failures, respectively. Here, the third fiber failure case is the worst one because its affected λ-bands are imposed on fewer living feeder fiber cables and the mean distance of the protection paths they traverse is longer. As shown in the figure, the communication services in both failure cases can be recovered via rerouting of those affected λ-bands.

4. EXPERIMENTAL SETUP AND RESULTS

To demonstrate the feasibility of the SRBA, we set up an experimental network as shown in Figure 7. In the downstream

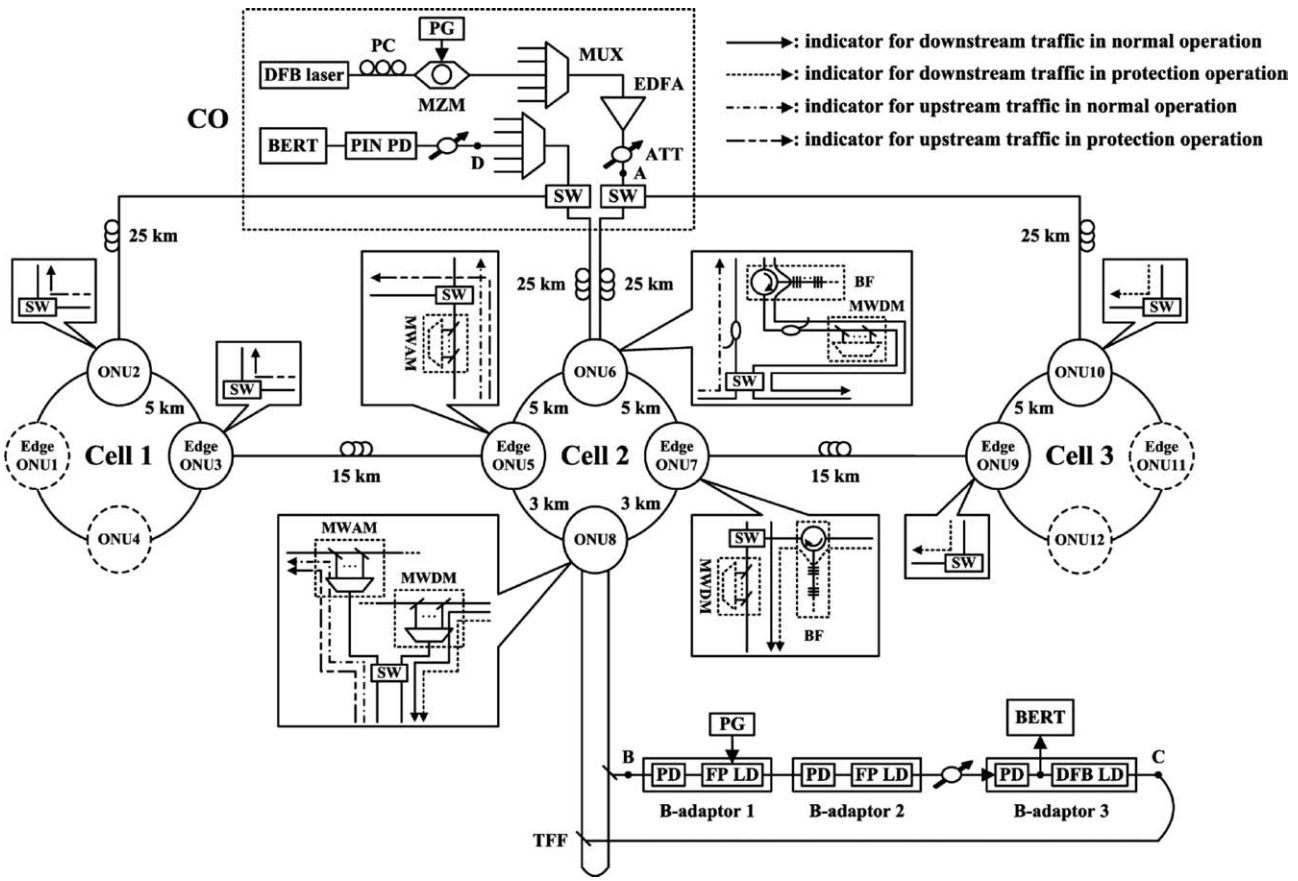

Figure 7 Experimental setup to demonstrate the feasibility of SRBA

direction, a tunable DFB laser with center wavelength of 1550.34 nm is externally modulated by a 1.25 Gb/s nonreturn-to-zero pseudo-random binary sequence data signal with 2^{31}- to 1-word length from a pattern generator. The optical-modulated signal generated from the Mach-Zehnder modulator is sent through a 1 × 8 AWG multiplexer, an EDFA, and a variable optical attenuator. The optical attenuator prevents the downstream signal from being nonlinearly amplified. In this experiment, the destination ONU8 of the downstream signal is located in the cell 2, as shown in Figure 7. Under normal operation, the optical signal of interest is delivered to the cell 2 directly via a 25-km single-mode fiber link. Once the feeder fiber link is removed to simulate the fiber cut scenario, it is switched to the neighboring cell 3.

Under the normal mode, the downstream signal first arrives at the ONU6, wherein it is dropped to a corresponding receiving fiber by means of a λ-band filter and a 10/90 fiber coupler and is sent through a multiwavelength drop multiplexer and an optical switch. Then, it goes through two sections of single-mode fiber links, the edge ONU7, and is finally received by a TFF of its destination ONU8. Under the protection mode, however, the optical signal is switched from the ONU10 to the edge ONU9 over a 5-km fiber link. Afterward, it is sent to the cell 2 in which its destination ONU8 is located via a 15-km fiber link. Within the edge ONU7 of cell 2, it is dropped by a BF and then is switched to the entity of edge ONU7. It can be seen that the optical signal of interest is drawn into the foregoing primary receiving lightpath, and naturally is dropped by the ONU8 as well.

Through a 1 × 8 AWG multiplexer and an optical switch inside the ONU8, the optical signal over the primary or backup receiving path is forwarded to the attached bus subnet. In the B-adaptor 1 of the subnet, the optical downstream signal is first converted to electrical by a PIN photodetector, and then is transmitted by a 1530-nm FP-LD module. The signal regeneration is repeated in the following B-adaptor 2. Finally, the resulting electrical data signal is sent to a bit-error-rate test set (BERT). The optical transmission losses from point A to B via the primary and backup downstream paths are 18.94 and 21.58 dB, respectively.

In the upstream direction, an identical 1.25 Gb/s RF data signal is used to directly modulate the 1530 nm FP laser inside B-adaptor 1. The resulting upstream signal is regenerated in B-adaptor 2, and is received by the PIN photodiode in B-adaptor 3. Next, the generated electrical data signal is transmitted by the coarse wavelength-division multiplexed 1550.34-nm DFB-LD module inside B-adaptor 3, and is forwarded to the ONU8 over a TFF. Within ONU8, the optical signal is switched to a multiwavelength add multiplexer (MWAM) and is then added to a 3-km single-mode fiber via this MWAM. Subsequently, it goes through the 3-km fiber link and arrives at the edge ONU5.

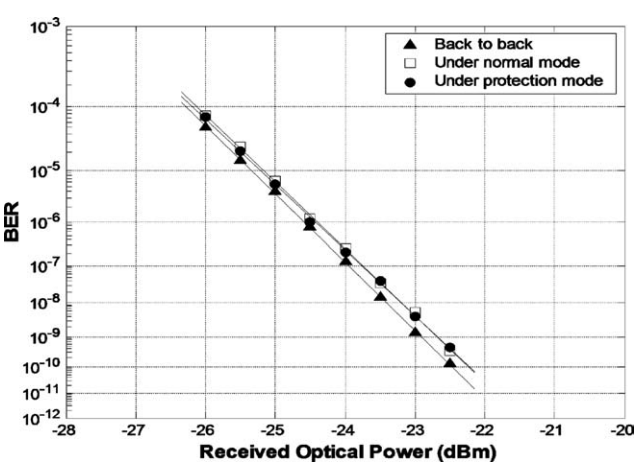

Figure 8 Downstream BER curves measured at the PIN-PD output in B-adaptor 3 and under the back-to-back, normal, and protection modes

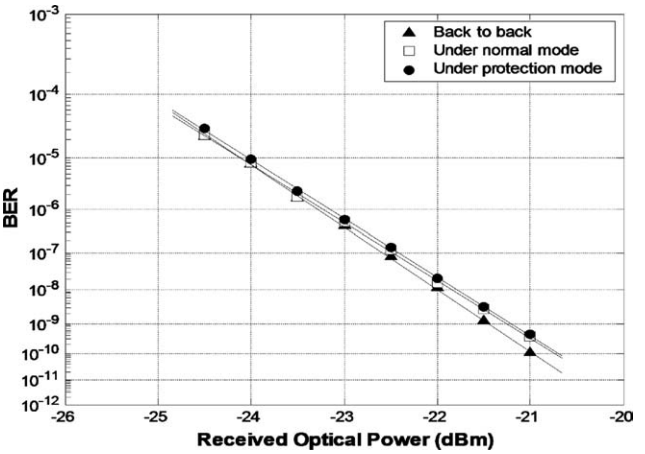

Figure 9 Upstream BER curves measured at the PIN-PD output in CO and under the back-to-back, normal, and protection modes

Under the normal condition, the upstream signal passes through the edge ONU5, a 5-km single-mode fiber, the ONU6, and then it goes to the CO via a 25-km feeder fiber link. Within the CO, it travels through a switch, a 1 × 8 AWG demultiplexer, a variable optical attenuator, a PIN photodetector, and is finally measured by a BERT. Although the fiber link between the CO and ONU6 is intentionally disconnected to simulate the fiber failure, the upstream signal is rerouted from edge ONU5 to CO, which signal track is illustrated as follows. First, at edge ONU5, it is switched to the cell 1 via a single-mode fiber of 15 km. Next, the optical signal goes through an edge switch inside ONU3, a 5-km single-mode fiber, and a switch in ONU2, as shown in Figure 7. After traversing a 25-km fiber link, it is switched to the primary transmitting path. The optical transmission losses from Point C to D via the primary and backup upstream paths are 18.24 and 21.88 dB, respectively.

Figure 8 shows the measured BER curves under the back-to-back, the 33-km normal, and the 48-km protection downstream transmission conditions versus the received optical power. They are all monitored at the output of the PIN-PD module in B-adaptor 3. In the downstream experiment, the optical signal power measured at Point A is 11 dBm, and the receiver sensitivity for Case 1 at BER = 10^{-9} is −23 dBm. At the BER of 10^{-9}, the induced power penalties in Case 2 and Case 3 relative to Case 1 are both less than 0.25 dB, as shown in Figure 8. Accordingly, the optical power margins of the downstream channels in Case 2 and Case 3 are 14.81 (11 − 18.94 − 0.25 + 23) and 12.17 (11 − 21.58 − 0.25 + 23) dB, respectively.

Figure 9 demonstrates the measured BER curves under the back-to-back, the 33 km normal, and the 48 km protection upstream transmission conditions versus the received optical power. They are all monitored at the output of the PIN receiver within CO. In the upstream experiment, the transmitted optical power of the 1550.34-nm DFB laser in B-adaptor 3 (measured at Point C) is 5 dBm, and the receiver sensitivity for Case 1 at BER= 10^{-9} is −21.5 dBm. At the BER of 10^{-9}, the induced power penalties in Case 2 and Case 3 relative to Case 1 are less

than 0.24 and 0.25 dB, as shown in Figure 9. Accordingly, the optical power margins of the upstream channels in Case 2 and Case 3 are 8.02 (5 − 18.24 − 0.24 + 21.5) and 4.37 (5 − 21.88 − 0.25 + 21.5) dB, respectively.

5. CONCLUSIONS

This work develops a novel SRBA for WDM regional access networks with high capacity and excellent reliability. The delta-star structure on the top level markedly reduces the difficulty and expense in network deployment as compared with conventional star networks, whereas its weakness in reliability is overcome by the self-healing function of the middle-level ring network. In our design, the ring network is divided into several delta regions, where the traffic load inside each region is almost unified for minimizing the backup resources required in case of fiber break(s). Moreover, the special cell structure cooperated with the λ-band scheme are introduced into the WDM access network to efficiently manage wavelength carriers used. The full-path protection capability of the proposed network is achieved with those APS systems installed in all the component ONUs. On the bottom level, the cascade of B-adaptors in each bus subnet enables easy signal regeneration; thereby, a large number of end users can be served. Finally, the transmission and recovery of the 1.25 Gb/s up/downstream signal flow under normal and protection networking modes have been experimentally demonstrated and characterized. The experimental results reveal that, in terms of reliability and flexibility, the proposed hybrid SRBA is a promising candidate for future high-capacity WDM access networks.

REFERENCES

1. M. Herzog, M. Maier, and A. Wolisz, RINGOSTAR: An evolutionary AWG-based WDM upgrade of optical ring networks, J Lightwave Technol 23 (2005), 1637–1651.
2. D.P. Shea and J.E. Mitchell, A 10-Gb/s 1024-way-split 100-km long-reach optical-access network, J Lightwave Technol 25 (2007), 685–693.
3. W.P. Lin, A cost-effective passive optical network based on multiple-optical-subcarrier multiplexing, Microwave Opt Technol Lett 12 (1996), 277–279.
4. A.A.M. Saleh and J.M. Simmons, Architectural principles of optical regional and metropolitan access networks, J Lightwave Technol 17 (1999), 2431–2448.
5. J. Zheng and H.T. Mouftah, Routing and wavelength assignment for advance reservation in wavelength-routed WDM optical networks, Proc IEEE ICC'02 5 (2002), 2722–2726.
6. M.-J. Li, M.J. Soulliere, D.J. Tebben, L. Nederlof, M.D. Vaughn, and R.E. Wagner, Transparent optical protection ring architectures and applications, J Lightwave Technol 23 (2005), 3388–3403.
7. F.-T. An, K.S. Kim, D. Gutierrez, S. Yam, E. Hu, K. Shrikhande, and L.G. Kazovsky, SUCCESS: A next-generation hybrid WDM/TDM optical access network architecture, J Lightwave Technol 22 (2004), 2557–2569.
8. I. Sankawa, F. Yamamoto, Y. Okumura, and Y. Ogura, Cost and quantity analysis of passive double-star optical-access-network facilities for broadband service multiplexing, J Lightwave Technol 24 (2006), 3625–3634.
9. X.-F. Sun, Z.-X. Wang, C.-K. Chan, and L.-K. Chen, A novel star-ring protection architecture scheme for WDM passive optical access networks, Proc OFC'05 3, 2005, paper JWA53.
10. T.-J. Chan, C.-K. Chan, L.-K. Chen, and F. Tong, A self-protected architecture for wavelength-division-multiplexed passive optical networks, IEEE Photon Technol Lett 15 (2003), 1660–1662.
11. M. Scheutzow, M. Maier, M. Reisslein, and A. Wolisz, Wavelength reuse for efficient packet-switched transport in an AWG-based metro WDM network, J Lightwave Technol 21 (2003), 1435–1455.
12. N. Nadarajah, E. Wong, M. Attygalle, and A. Nirmalathas, Protection switching and local area network emulation in passive optical networks, J Lightwave Technol 24 (2006), 1955–1967.
13. T.S. Rappaport, Wireless communications, principles and practice, Prentice Hall, New Jersey, 1996.

COMPACT DUALBAND BANDPASS FILTER WITH TWO TRANSMISSION ZEROS USING DUAL-MODE MICROSTRIP RESONATOR AND TAPPED-LINE GEOMETRY

Tae-Soon Yun,[1] Sun-Kuk Noh,[1] Hyung-Jong Kim,[1] Euy-Kyo Oh,[1] Hong-Min Son,[1] and Jong-Chul Lee[2]

[1] Department of Radio Mobile Communication Engineering, Honam University, 330 Eodeungno, Gwangsan-gu, Gwangju, Korea; Corresponding author: easteryun@gmail.com

[2] Department of Electronics Convergence Engineering, Kwangwoon University, 447-1 Wolgye-dong, Nowon-gu, Seoul 139-701, Korea

Received 16 April 2010

ABSTRACT: *In this article, the dualband bandpass filters (BPFs) using dual-mode resonator are designed and implemented. Also, the J-inverter is investigated as function of the impedance and the electrical length of the open-stub in the dual-mode $\lambda_g/2$ microstrip resonator. Especially, the dualband BPFs using dual-mode resonator are realized by the stepped impedance resonator (SIR) structure and have good out-of-band performance as the inverter is alternating by the coupling structure and tapped-line geometry. The first transmission zero of the dualband BPFs is made by the dual-mode resonator and the second transmission zero is defined by the open-stub of the tapped-line geometry as a function of J-inverter. The dualband BPF using dual-mode resonator with two transmission zeros shows the insertion losses of 1.92 and 1.71 dB at the center frequency of 2.42 and 5.65 GHz, respectively.* © 2010 Wiley Periodicals, Inc. Microwave Opt Technol Lett 53:108–111, 2011; View this article online at wileyonlinelibrary.com. DOI 10.1002/mop.25627

Key words: *transmission zero; dual-mode; stepped impedance resonator; tapped-line; bandpass filter*

1. INTRODUCTION

In the last decade, a microstrip bandpass filter (BPF) using a half-wavelength ($\lambda_g/2$) microstrip transmission line resonator with a tap connected open-stub as shown in Figure 1(a) is developed and reported for dual-mode resonance and the transmission zero [1–4]. Generally, to obtain high selectivity of BPFs, more resonators are used or the elliptic-function response is used such as open-loop resonators and ring resonators [5]. The elliptic-function BPFs have transmission zeros and can obtain high selectivity by using smaller number of resonators. Otherwise, because it has transmission zero at one side of the passband by the electrical length of an open-stub, high selectivity can be more easily achieved for a BPF using a dual-mode $\lambda_g/2$ microstrip resonator. Usually, the *J*-inverter of the dual-mode BPF is realized by the coupling structure, whereas the value of the *J*-inverter is rarely researched. In our work, the *J*-inverter is investigated as functions of the electrical length, the impedance of the open-stub, and the ripple characteristic. Also, for the dualband application, the stepped impedance resonator (SIR) is imported in the dual-mode microstrip resonator as shown in Figure 1(b). The spurious response of the SIR structure can be controlled by the stepped impedance ratio [6–7]. Because the transmission zero is not happened as using the first spurious response of the